Electrohydrodynamic Flow and its Effect on Ozone Transport in Corona Radical Shower Reactor

Jaroslaw Dekowski, Jerzy Mizeraczyk, Marek Kocik, Mirosław Dors, Janusz Podliński, Seiji Kanazawa, *Member, IEEE*, Toshikazu Ohkubo, *Member, IEEE*, and Jen-Shih Chang, *Senior Member, IEEE*

***Abstract*—New arguments supporting the supposition that the ozone is transported along a corona discharge radical shower (CDRS) reactor by the electrohydrodynamic (EHD) flow are presented. The arguments are based on the analysis of the corona discharge, which is a precursor of the EHD flow in the CDRS reactor, and on the measurements of velocity field of the EHD flow in the CDRS reactor by the particle image velocimetry (PIV). The obtained velocity flow structures and the possible causes of the ozone transport in the CDRS, i.e., diffusion, additional gas flow, EHD flow, and convection by the main flow, were discussed basing on the conservation equations for the EHD flow. The discussion showed that the EHD flow plays a dominant role in the ozone transport. This is also supported by the results of a simple phenomenological model for one-dimensional description of EHD-induced ozone transport in the CDRS reactor. The results of the computer simulation based on this model explained the main features of the measured ozone distribution in the CDRS reactor, establishing the EHD flow as the main cause of the ozone transport from the discharge region upstream, i.e., against the main flow.**

***Index Terms*—Corona discharge radical shower (CDRS), electrohydrodynamic flow, particle image velocimetry.**

I. Introduction

NONTHERMAL plasma techniques [1]–[3] have become an important tool for controlling the emission of various gaseous pollutants, such as acid gases (SO_x, NO_x, HCl, etc.), greenhouse gases (CO_x, N_xO_y, para-fluorocarbons, etc.), ozone depletion gases (freons, halons, etc.), volatile organic compounds (VOCs, e.g., toluene, xylene, etc.), and toxic gases (Hg, dioxins, etc.). The main advantages of the nonthermal plasma techniques are small space volume, low cost, high pollutant removal, and energy efficiencies.

Recently, Ohkubo *et al.* [4], [5] and Kanazawa *et al.* [6] measured the two-dimensional distribution of ground-state NO density by the laser induced fluorescence (LIF) in needle-to-plate and corona discharge radical shower (CDRS) nonthermal plasma reactors, respectively, showing that the concentration of NO molecules decreased not only in the streamer corona discharge and downstream regions of the reactor but also upstream of the discharge region. The reason for the NO removal in the upstream region of the discharge was not clear. However, the results of numerical and experimental investigations [7]–[10] on the electrohydrodynamic (EHD) secondary flow (ionic wind) in electrostatic precipitators allow us to make a supposition [11] that the EHD flow may be capable of transporting the long-live active species (e.g., ozone) from the discharge region to the upstream region of nonthermal plasma reactors. If so, the long-live active ozone (or other species) produced in the discharge region could be transported by the EHD flow into the upstream region to oxidize or reduce NO molecules and efficiently decrease their concentration there, as was experimentally observed in [4]–[6]. Mizeraczyk *et al.* [12] conducted an experiment to elucidate the effect of the EHD flow on ozone transport in the CDRS reactors. By measuring the ozone distribution along the CDRS reactor and visualizing the EHD flow in the CDRS reactor, they confirmed the existence of a strong EHD flow in the CDRS reactor which may easily distribute the ozone inside the reactor, even far into the upstream direction of the reactor.

CDRS reactors have been recently proved to be one of the most efficient nonthermal plasma reactor systems used for NO_x removal [13]–[15]. In a CDRS reactor, an electrode with one or several nozzles is used for additional gas (NH_3, CH_4, etc.) injection across the corona discharge zone into the main flue gas flow. Due to the additional gas injection, the corona discharge produces active species such as NH, NH_2, CH, CH_2, etc., which enhance the removal of NO_x. The performance of the CDRS reactors can be also improved by the transport of the long-life species, caused by the EHD secondary flow, as was suggested in [12]. However, the suggested importance of EHD flow regarding the long-life species transport has not been supported sufficiently by evidence.

In this paper, new arguments for the ozone molecule transport by the EHD flow along a CDRS nonthermal plasma reactor are presented. The arguments were obtained from the analysis of the properties of the corona discharge, which is a precursor of the EHD flow in the CDRS reactor, and of the velocity field of the EHD flow in the CDRS reactor, measured by the particle image velocimetry (PIV). The analysis was supported by a simple phenomenological model of the ozone transport in the CDRS reactor.

Manuscript received August 31, 2003; revised January 20, 2004. This work was supported in part by the Foundation for Polish Science (Fundacja na Rzecz Nauki Polskiej, subsidy 8/2001), the State Committee for Scientific Research under Grant KBN PB 1756/T10/01/21, and the Canadian-Japanese-Polish Scientific Cooperation on Nonthermal Plasma Applications.

J. Dekowski, J. Mizeraczyk, M. Kocik, M. Dors, and J. Podliński are with the Centre for Plasma and Laser Engineering, Institute of Fluid Flow Machinery, Polish Academy of Sciences, 80-231 Gdańsk, Poland (e-mail: kwisatz@imp.gda.pl; jmiz@imp.gda.pl; kocik@imp.gda.pl; mdors@imp.gda.pl; janusz@karol.imp.gda.pl).

S. Kanazawa and T. Ohkubo are with the Department of Electrical and Electronic Engineering, Oita University, Oita 870-1192, Japan (e-mail: skana@cc.oita-u.ac.jp; tohkubo@cc.oita-u.ac.jp).

J. S. Chang is with the Department of Engineering Physics, McMaster University, Hamilton, L8S 4M1 ON, Canada (e-mail: changj@mcmaster.ca).

Digital Object Identifier 10.1109/TPS.2004.828458

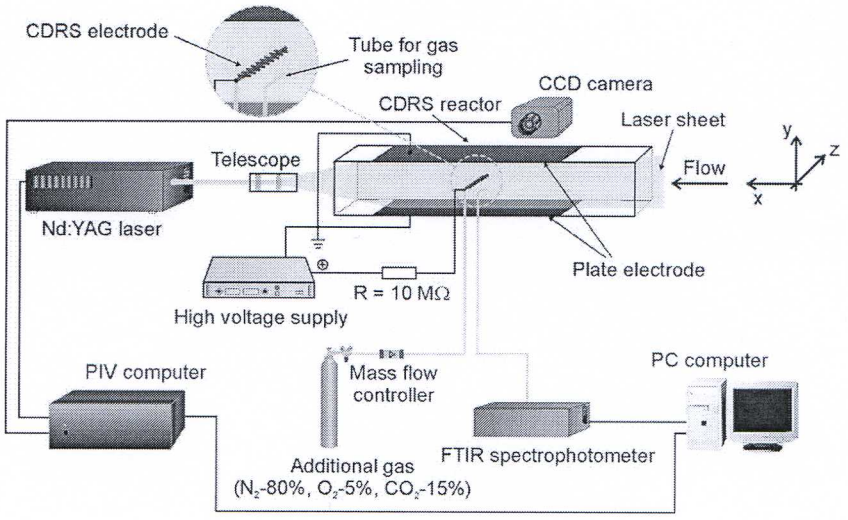

Fig. 1. Experimental setup.

In addition to the fundamental interest in the species transport in the nonthermal plasma reactors, this investigation is related to the topical questions of the nonthermal plasma technology for gaseous pollutant abatement:

1) how (if at all) the corona discharge itself and the no-discharge region (the part of the reactor not covered by the discharge) are involved in the reduction and/or oxidation of the gaseous pollutants in the nonthermal plasma reactors;
2) how accurately the present chemical kinetics modeling of the gaseous pollutant removal processes caused by the corona discharge (e.g., [16]–[18]), which neglects involvement of the no-discharge region, depicts the real phenomena in the nonthermal plasma reactors, and how the current modeling state-of-the art can be useful for optimising the performance of the nonthermal plasma reactors.

II. Experimental Apparatus

A schematic of the experimental apparatus used for measurement of the flow velocity fields in the CDRS reactor is shown in Fig. 1. The reactor was an acrylic box of a rectangular geometry (100 × 200 × 1000 mm) as used by Mizeraczyk *et al.* [12] when measuring the ozone distribution in the CDRS. A stainless-steel pipe (4 mm in diameter) with 18 stainless-steel nozzle electrodes (1.5-mm outer diameter, 1-mm inner diameter, 5-mm length), soldered into the pipe as shown in Fig. 2, was used as the CDRS electrode. It was placed in the middle of the reactor, half way between two grounded parallel plate electrodes (200 × 600 mm). Positive polarity dc high voltage was applied through a 10-MΩ resistor to the CDRS electrode. The operating voltage was varied from 0 to 31 kV to develop a stable streamer corona discharge from each electrode nozzle to the plate electrodes. The discharge was operated at room temperature under atmospheric pressure.

Two flows, the main and the additional, were established in the reactor. The main gas (ambient air) flowed along the reactor, driven by an induced fan. The mean velocity of the

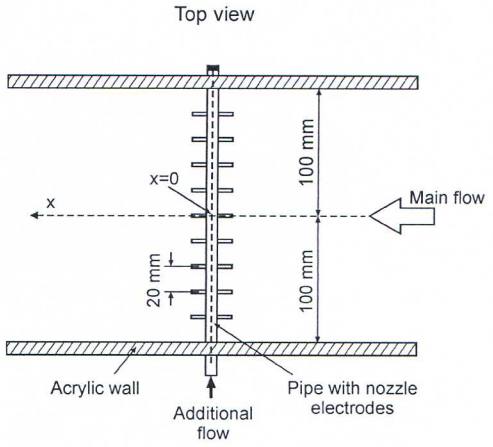

Fig. 2. Top-view schematic of the pipe with nozzle electrodes. Nozzle electrodes are shown oversized.

main gas flow was varied from $U_s = 0$ to $U_s = 0.8$ m/s, which corresponds to the flow change from laminar to transitional (Reynolds number varied from Re = 600 to 2660 for $U_s = 0.18$ m/s and $U_s = 0.8$ m/s, respectively). The standard deviation of the mean main gas flow velocity was ±4%, as measured with the PIV. The additional gas ($N_2 : O_2 : CO_2 = 80\% : 5\% : 15\%$) was injected through the nozzles into the main gas flow with a flow rate varied from 0.25 to 1.5 l/min (nozzle outlet gas velocity ranged from 0.3 to 1.8 m/s, corresponding to Re = 30–180, respectively). The presence of CO_2 (15%) stabilized streamer corona discharge mode, preventing glow and spark discharge modes [19].

Fig. 1 shows also a cylindrical plastic sampling probe (1 mm in diameter), through which the working gas was sucked into a calibrated FTIR spectrophotometer, as used by Mizeraczyk *et al.* [12] for measuring the ozone concentration along the x axis placed 1 cm below the nozzle electrode in the CDRS reactor (Fig. 2).

The flow velocity fields in the CDRS reactor were measured using the PIV method. The PIV equipment consisted of a twin second harmonic Nd—YAG laser system ($\lambda = 532$ Nm, pulse

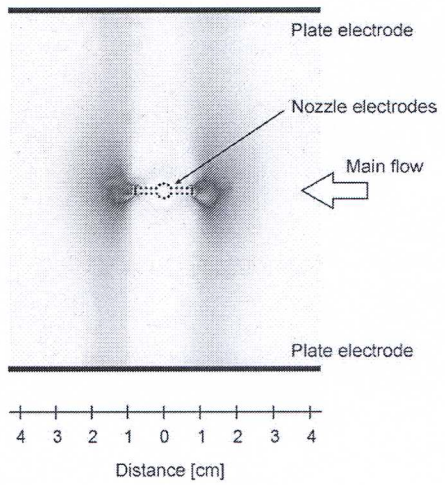

Fig. 3. Typical image (side view) of the streamer corona discharge in the CDRS reactor. Main gas (air) flow velocity—$U_s = 0.18$ m/s, additional gas [$N_2(80\%)$: $O_2(5\%)$: $CO_2(15\%)$] flow rate $Q_a = 0.5$ l/min, applied voltage $V = 28.2$ kV, averaged total corona discharge current $I = 150$ μA, and exposure time of the CCD camera is 8 s.

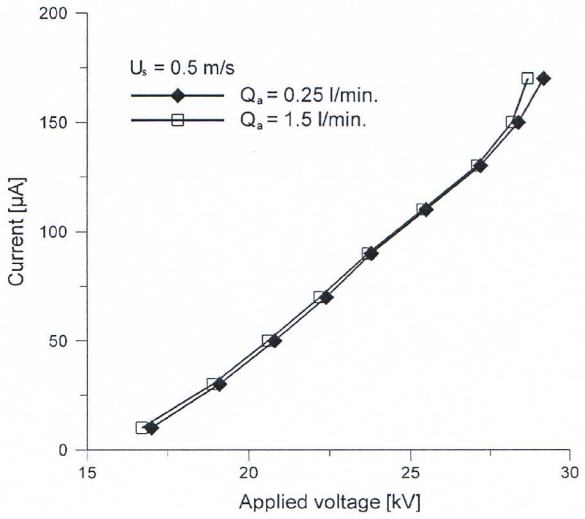

Fig. 4. Time-averaged current–voltage characteristics of the positive dc streamer corona discharge in the CDRS reactor for various additional gas [$N_2(80\%)$: $O_2(5\%)$: $CO_2(15\%)$] flow rates Q_a. Main gas (air) velocity $U_s = 0.5$ m/s.

energy 50 mJ), imaging optics (cylindrical telescope), charge-coupled device (CCD) camera, image processor (Dantec PIV 1100), and PC computer (Fig. 1). A laser sheet of thickness of 1 mm, formed from the Nd–YAG laser beam by the cylindrical telescope, was introduced into the CDRS reactor as a plane perpendicular to the plate electrodes, passing through the middle nozzles (at $x = 0$ in Fig. 2). Seed particulate (cigarette smoke), being expected to follow the flow, was added to the main gas for scattering the laser-sheet light. The particle images were recorded by the Kodak Mega Plus ES 1.0 CCD camera, which could capture two images with a minimum time separation of 2 μs. The CCD camera active element size was 1008×1018 pixels. The captured images were transmitted by the Dantec PIV 1100 image processor to the PC computer for digital analysis to obtain the velocity field maps in the CDRS reactor.

We assumed that the flow in the CDRS reactor is symmetric regarding the horizontal plane (parallel to the plate electrodes) passing through the discharge electrode. Therefore, in this experiment, the PIV measurement area was limited to the lower half of the CDRS reactor.

The velocity field maps presented in this paper are composed of four adjacent velocity fields, each of an area of 75×75 mm. Since it was found in this experiment that the flow structure pattern in the CDRS reactor is unsteady, the majority of the velocity field maps resulted from the averaging of 100 measurements, i.e., the presented velocity maps are time averaged, unless otherwise stated.

III. Experimental Results

A. Discharge Characteristics

When observed with the naked eye or recorded with a CCD camera having a long exposure time, the discharge from the CDRS electrodes exhibits a flame-like pattern as shown in Fig. 3. However, the images recorded in [6] with a short exposure-time ICCD camera showed that the discharge in the CDRS reactor consists of branching streamers, each starting from the tip of the nozzle electrode and propagating toward the plate electrodes, eventually bridging the electrode gap. In the present discharge electrode design (Fig. 2), the streamer starting point on the tip of the nozzle directed upstream was 14 mm apart from that directed downstream. The volume occupied by the streamers increased with increasing discharge current. We estimate that at a total discharge current of $I = 150$ μA, all the streamers from the one side of the CDRS electrode (upstream or downstream), when bridging the electrode gap, covered the grounded electrode with an area which was roughly a rectangle having a length equal to that of the CDRS electrode (200 mm) and a width of 10 mm. Therefore, all the streamers formed a kind of narrow curtain across the reactor at the upstream and downstream sides, which the main gas had to pass through.

In the typical CDRS reactors, when the main gas is a N_2 : O_2 : CO_2 : NO mixture and the additional gas is a mixture of N_2 : NH_3, the time-averaged current–voltage characteristics of the discharge are hardly affected by the presence of the additional flow; however, they are influenced at high operating voltages by the presence of NH_3 molecules, as shown in [13]. In the present CDRS reactor, the streamer corona discharge onset occurred when the applied voltage increased above about 15 kV (Figs. 4 and 5). Then, the discharge current increased monotonically with increasing voltage. No essential difference in the time averaged current–voltage characteristics was observed when the additional gas flow rate or the main gas flow velocity was varied from 0.25 to 1.5 l/min or from 0 to 0.8 m/s, respectively. Since there was no NH_3 additive in the additional gas, the presented time-averaged current–voltage characteristics do not exhibit the peculiarities observed in [13].

B. Spatial Distribution of Ozone Concentration

In general, the active species produced around the electrodes by the streamer corona discharge can be transported from their origin into both the downstream and upstream regions of the CDRS reactor by the diffusion and additional gas flow from all

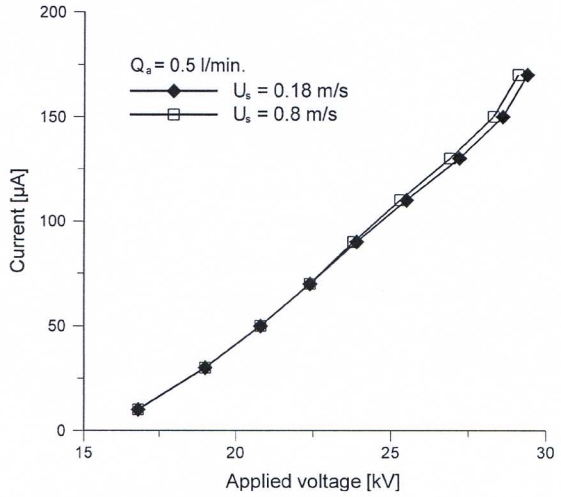

Fig. 5. Time-averaged current–voltage characteristics of the positive dc streamer corona discharge in the CDRS reactor for various main gas (air) flow velocities U_s. Additional gas [$N_2(80\%)$: $O_2(5\%)$: $CO_2(15\%)$] flow rate $Q_a = 0.5$ l/min.

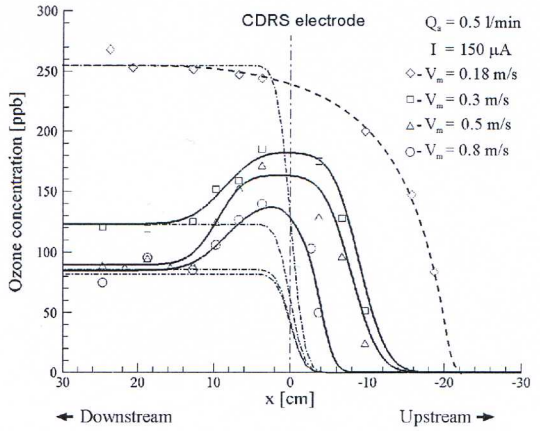

Fig. 6. Time-averaged ozone concentration distributions along the CDRS reactor during the positive dc streamer corona discharge for various main gas (air) flow velocities U_s. Dotted lines are experimental data (after Mizeraczyk *et al.* [12]). Solid lines are calculation results based on the simplified model of one-dimensional ozone transport which involves the EHD flow. Dashed–dotted lines show calculation results based on the simplified model without the EHD and additional gas flows. Dashed line fits the experimental points for $U_s = 0.18$ m/s. Ozone concentrations were measured along x axis, placed along the reactor 1 cm below the discharge electrode (see Fig. 2). Additional gas [$N_2(80\%)$: $O_2(5\%)$: $CO_2(15\%)$] flow rate $Q_a = 0.5$ l/min, averaged total discharge current $I = 150$ μA.

the nozzles and by the electrohydrodynamic (EHD) secondary flow as suggested in [12]. They can be also transported downstream by convection of the main gas flow. When a steady state is established in the CDRS reactor, a spatial distribution of the active species is settled as the net result of the production of active species and their transport.

Fig. 6 shows the typical time-averaged ozone concentration distributions along the CDRS reactor for various main gas flow velocities from 0.18 to 0.8 m/s, as measured by Mizeraczyk *et al.* [12]. The main features of the ozone concentration distributions in the CDRS reactor are as follows.

1) Ozone molecules are present in both the downstream and upstream regions of the CDRS reactor, assuming the position of the discharge electrode as a reference.

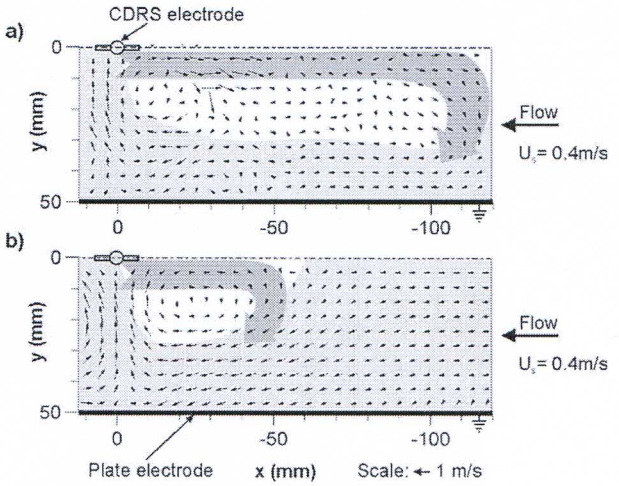

Fig. 7. (a) Instantaneous and (b) time-averaged flow velocity fields in the lower half of the CDRS reactor at a main flow velocity $U_s = 0.4$ m/s (observation plane crossed the middle electrode nozzles; see Fig. 2). Positive voltage polarity, averaged total discharge current $I = 150$ μA, and additional gas flow rate $Q_a = 0.5$ l/min.

2) The ozone concentration exhibits a maximum around the discharge zone due to the ozone production and decreases when moving upstream and downstream, for the main gas flow velocities higher than 0.18 m/s. At the lowest main gas flow velocity tested (0.18 m/s), the ozone concentration distribution does not exhibit any maximum around the discharge zone and it does not decrease when moving downstream.
3) The ozone penetration length upstream depends on main gas flow velocity. It is shorter at higher main gas flow velocities because the role of the main gas convection in the ozone molecule transport increases. The ozone molecules are found upstream as deep as about 20 cm from the discharge electrode, at a main gas flow velocity of 0.18 m/s. At a main gas flow rate of 0.8 m/s, the ozone molecules penetrate only a few centimeters upstream.

From the constant ozone concentration at the reactor exit (i.e., for $x > 30$ cm downstream, Fig. 6) it was possible to estimate the ozone production rate per one nozzle electrode at 1.33×10^{15} molecules/s (averaged for all main gas velocities at a time-averaged total discharge current of 150 μA).

C. Flow Velocity Field Structures

The analysis of instantaneous flow velocity field patterns measured in the CDRS with the PIV showed that at constant flow and discharge parameters the upstream flow patterns varied stochastically, exhibiting a cyclic regularity. The obtained instantaneous velocity field patterns confirmed the existence of strong vortexes in the CDRS reactor caused by the EHD force. However, the position of the upstream vortexes along the reactor was not stable. The vortex, originally formed in the vicinity of the CDRS reactor, moved more or less regularly from the near-electrode region toward the upstream region; after reaching its furthest position there, it returned back toward the electrode. Fig. 7(a) shows the furthermost instantaneous vortex position in the upstream region of the

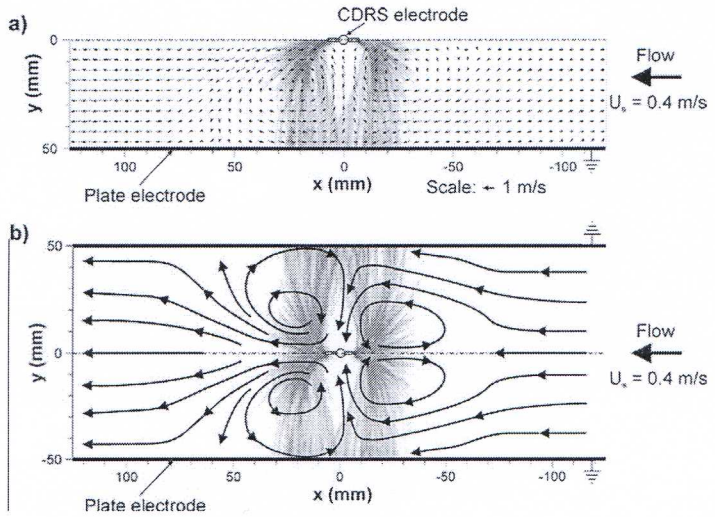

Fig. 8. (a) Time-averaged flow velocity field and (b) streamlines of the gas flow with inserted image of the streamers in the CDRS reactor at a main flow velocity $U_s = 0.4$ m/s observation plane crossed the middle electrode nozzles; see Fig. 2). Positive voltage polarity, averaged total discharge current $I = 150$ μA, additional gas flow rate $Q_a = 0.5$ l/min. Streamer image: ICCD camera, exposure time 0.6 ms, and average of 100 images.

reactor. The "to and fro" movement of the vortex exhibited an oscillatory character with stochastic fluctuations. On the other hand, the time-averaged flow velocity field pattern shows the most probable position of the vortex [Fig. 7(b)]. The near-electrode positioning of the time-averaged vortex [as seen in Fig. 7(b)] suggests that the instantaneous vortex occupies that region more frequently than the other regions.

Fig. 8(a) shows the time-averaged velocity field map for the lower half of the CDRS reactor, and Fig. 8(b) shows the corresponding streamlines of the gas flow, inferred from Fig. 8(a), both for the whole CDRS reactor.

The direction of rotation of the electrohydrodynamicaly caused vortexes is opposite to that observed in ESP models with smooth wire discharge electrode (e.g., [10]). As seen in Figs. 7 and 8, the gas in the upstream (downstream) vortex moves from the electrode nozzle upstream against the main flow (downstream along the main flow), then separates into two flows, each of which turns toward the corresponding plate electrode; after passing along the plate electrode, each flow returns back to the CDRS electrode. In contrast, when the smooth wire electrode is used the gas is electrohydrodynamically forced to move from the smooth wire electrode directly toward the plate electrodes, then it flows along the plate electrodes and turns to return to the wire electrode. As a result, the near wire electrode vortexes revolve in the opposite direction to those formed near the CDRS electrode.

It was found that the EHD flow structures depend on velocity of the main flow. At lower main flow velocities, the near-electrode time-averaged vortexes are stronger and better pronounced than at higher velocities. This is caused by the dominance of the EHD forces over the inertial forces at low main flow velocities (see Section V-C). Without the main flow ($U_s = 0$) or at a relatively low main flow velocity of 0.2 m/s, the time-averaged vortexes formed at both sides of the CDRS electrode are strong. At higher main flow velocities (0.4–0.6 m/s), the time-averaged vortexes at the upstream side of the discharge electrode, although smaller, still are pronounced (see Figs. 7 and 8). Due to the strong vortexes near the CDRS electrode, the main flow changes its route. It does not move uniformly through the whole cross section of the reactor duct but it separates into two flow (Fig. 8). Each of them passes between the corresponding upstream vortex and the plate electrode, then vigorously turns toward the CDRS discharge electrode to form a single flow again which passes between both downstream vortexes and eventually expands at the CDRS reactor exit. This complex flow structure together with the upstream and downstream vortexes obviously must influence the distribution of the gas molecules, including ozone, in the CDRS reactor.

IV. Conservation Equations for EHD Flow

For a dielectric fluid, such as that in the CDRS reactor, the EHD-induced flow velocity does not exceed Mach number $M = 0.2$. Therefore, the subsonic incompressible flow is considered. It is also assumed that the mean free path of the fluid particle is much shorter than the characteristic length of the reactor duct; hence, the continuum fluid flow mechanics is considered. The discussion is limited to the Newtonian fluid without the viscous dissipation heating of the fluid and natural convection.

Under these assumptions, the mass, momentum, ion, and molecule conservation equations in the gas flow in the presence of the electric field can be expressed as follows [20]:

i) **Mass conservation**

$$\frac{\partial \rho}{\partial t} + \nabla \cdot \left(\rho \cdot \vec{U}\right) = 0. \tag{1}$$

ii) **Momentum conservation**

$$\rho \frac{\partial \vec{U}}{\partial t} + \rho \left(\vec{U} \cdot \nabla\right) \vec{U} = -\nabla P + \vec{F}_{EB} + \mu_D \nabla^2 \vec{U} \tag{2}$$

where

$$\vec{F}_{EB} = \rho_i \vec{E} - \frac{1}{2}\left(\vec{E} \cdot \vec{E}\right) \nabla \varepsilon.$$

iii) **Ion transport equation**

$$-\frac{\partial N_i}{\partial t} = -S_i + \vec{U}\cdot\nabla N_i \pm \mu_i \nabla\cdot\left(N_i\vec{E}\right) - D_i\nabla^2 N_i. \quad (3)$$

iv) **Poisson's equation**

$$\nabla\cdot\vec{E} = -\frac{e}{\varepsilon}N_i \quad (4)$$

where $\vec{E} = -\nabla V$.

v) **Molecule transport equations**

for neutral molecules

$$-\frac{\partial N_n}{\partial t} = -S_n + \vec{U}\cdot\nabla N_n - D_n\nabla^2 N_n \quad (5)$$

and for charged molecules

$$-\frac{\partial N_c}{\partial t} = -S_c + \vec{U}\cdot\nabla N_c \pm \mu_c\nabla\cdot(N_c\vec{E}) - D_c\nabla^2 N_c \quad (6)$$

where ρ is the gas density, $\vec{U}$ is the gas flow velocity, t is the time, μ_D is the gas viscosity, P is the pressure, N is the ion or molecule number density, e is the elementary charge, ε is the dielectric constant, D is the diffusion coefficient, μ is the ion mobility, $\vec{E}$ is the electric field, V is the electric potential, S is the molecule source and sink term, subscript i refers to ions (summarized all ion species, $\rho_i = eN_i$), subscript n refers to the specific neutral molecule species, and subscripts c refers to the specific charged molecule species.

For the steady state, the nondimensional form of the conservation equations with the Poisson's and the charged particle transport equations become

$$\tilde{\nabla}\cdot\vec{u} = 0 \quad (7)$$

$$\vec{u}\cdot\tilde{\nabla}\vec{u} = -\tilde{\nabla}p + \frac{E_{\rm hd}}{\mathrm{Re}^2}n_i\vec{\eta} - \frac{Md}{2\mathrm{Re}^2}(\vec{\eta}\cdot\vec{\eta})\tilde{\nabla}\varepsilon_r + \frac{1}{\mathrm{Re}}\tilde{\nabla}^2\vec{u} \quad (8)$$

$$\mathrm{Re}Sc_i\vec{u}\cdot\tilde{\nabla}n_i \mp \tilde{\nabla}\left(n_i\tilde{\nabla}\phi\right) - \tilde{\nabla}^2 n_i = s_i \quad (9)$$

$$\tilde{\nabla}^2\phi = -(\mathrm{Db})^2(n_+ - n_-) = \tilde{\nabla}\vec{\eta} \quad (10)$$

$$\mathrm{Re}Sc_n\vec{u}\cdot\tilde{\nabla}n_n - \tilde{\nabla}^2 n_n = s_n \quad (11)$$

$$\mathrm{Re}Sc_c\vec{u}\cdot\tilde{\nabla}n_c \mp \tilde{\nabla}\left(n_c\tilde{\nabla}\phi\right) - \tilde{\nabla}^2 n_c = s_c \quad (12)$$

where the nondimensional variables are

$$\vec{u} = \frac{\vec{U}}{U_s},\quad n = \frac{N}{N_s},\quad \phi = \frac{eV}{kT},\quad \vec{\eta} = \frac{\vec{E}}{E_s},\quad \vec{j} = \frac{\vec{J}}{J_s}$$

$$p = \frac{P}{\rho U_s^2},\quad \varepsilon_r = \frac{\varepsilon}{\varepsilon_0},\quad s = \frac{D_S}{L_s^2 N_s},\quad \mathrm{Re} = \frac{U_s L_s}{\nu}$$

$$E_{\rm hd} = \frac{eN_sE_sL_s^3}{\rho\nu^2} = \frac{\sigma_sE_sL_s^3}{\rho\nu^2\mu_i} = \frac{J_sL_s^3}{\rho\nu^2\mu_i} = \frac{I_sL_s^3}{\rho\nu^2\mu_iA}$$

$$Sc = \frac{\nu}{D},\quad Md = \frac{\varepsilon_0E_s^2L_s^2}{\rho\nu^2},\quad Db = \frac{L_s}{\lambda_D},\quad \mathrm{Pe} = \mathrm{Re}Sc.$$

Here, subscript s refers to the characteristic quantities where U_s, N_s, E_s, J_s, I_s, L_s, and σ_s are the characteristic velocity, gas density, electric field, current density at the electrode, total current, length, and electric conductivity, respectively, ε_0 is the dielectric constant in vacuum, ε_r is the specific dielectric constant, A is electrode surface area, k is Boltzmann's constant, Re is Reynolds number, $E_{\rm hd}$ is the EHD number, Sc is the Schmidt number, Md is Masuda number, Db is Debye number, λ_D is Debye length $\left(\varepsilon kT/e^2N_s\right)^{1/2}$, Pe is Peclet number, and subscripts + and − refer to positive and negative ions, respectively.

To obtain detail flow profiles in the CDRS reactor, (7)–(12) must be solved, which is a difficult task. However, some properties of the plasma and the flow inside the CDRS reactor can be evaluated by Reynolds number Re, ion Schmidt number Sc, EHD number $E_{\rm hd}$, Debye number Db, and Masuda number Md. For the gaseous plasma flow in the CDRS reactor the specific dielectric constant $\varepsilon_r \cong 1$; hence, $\tilde{\nabla}\varepsilon_r \cong 0$. Therefore, the EHD induced secondary flow becomes dominant when $E_{\rm hd} \gtrsim \mathrm{Re}^2$ [(8)].

When $E_{\rm hd} \gtrsim \mathrm{Re}^2$, the following effects of the EHD force upon the fluid flow in nonthermal plasma reactors can be expected [9]–[11]:

1) micro and bulk convection in the form of EHD generated vortexes;
2) flow turbulence and instabilities;
3) particle entrainments.

The experimental results presented in Figs. 7 and 8 show the presence of the above-mentioned effects.

V. Ozone Transport

The investigation of Mizeraczyk *et al.* [12] showed that the ozone molecules (and likely other long-live active species) produced by the streamer corona discharge in the CDRS reactor are transported not only in the downstream direction, but also far upstream of the main flow (Fig. 6). In the case of the CDRS reactor, three factors can be considered responsible for the ozone transport upstream: the diffusion, additional flow (from the nozzles facing upstream), and EHD secondary flow directed upstream. The counteracting factor in the upstream region is the main flow convection which transports the ozone molecules downstream.

A. Diffusion

A comparison of the relative importance of the diffusion and the main flow convection regarding the ozone transport can be conducted by analyzing the dimensionless transport (11) for neutral molecules. Equation (11) shows that the ozone diffusion transport is comparable to the convection when $\mathrm{Re}Sc = \mathrm{Pe} \ll 1$, where Pe is the diffusion Peclet number for ozone molecule. The diffusion Peclet number for the presented CDRS reactor varies from $\mathrm{Pe} = 450$ at $U_s = 0.18$ m/s to $\mathrm{Pe} = 2000$ at $U_s = 0.8$ m/s. Therefore, it is clear that the molecular diffusion transport is negligible in comparison with the main flow convection. This means that the diffusion cannot be responsible for the ozone transport upstream. This conclusion was also confirmed by the numerical solution of a simplified convection-diffusion ozone transport equation without EHD and additional gas flow, as presented in Section V-D. The disagreement between the ozone concentration numerically calculated from the simple diffusion-convection transport equation and that measured experimentally (Fig. 6) confirms the neglible role of the diffusion in the ozone transport upstream.

B. Additional Gas Flow

The velocity of the additional gas flow at the nozzle outlet (about 0.6 m/s as calculated and measured by the PIV) is comparable with the main gas flow velocity (0.18 to 0.8 m/s). However, the flow rate of the additional gas upstream is 0.12–0.75 l/min only, while the main gas flow rate ranges from 216 to 960 l/min at main flow velocities from 0.18 to 0.8 m/s, respectively. Such a large mass of the main gas flow surpresses easily the additional gas jet from the electrode nozzles and quenches it in the vicinity of the nozzle (the jet extinguishes at a distance of 1.5 cm from the nozzle when the main flow velocity is as low as 0.18 m/s [12]). Therefore, although the effects of the additional gas flow and main gas flow can be comparable in the very close vicinity of the electrode nozzle, the additional gas flow cannot be responsible for the transfer of the ozone far into the upstream region of the CDRS reactor.

C. EHD Secondary Flow

The apparent importance of the additional gas flow in the close vicinity of the CDRS electrode nozzle, when compared with that of the main flow, is, however, overwhelmed by the strong EHD flows resulted from the applied voltage and the flow of ions formed around the CDRS electrode. Comparing the EHD force with the inertia force of the additional gas flow, both forces in the close vicinity of the CDRS electrode nozzle result in Reynolds and EHD numbers equal to $\mathrm{Re} = 59$ and $E_{\mathrm{hd}} = 198 \times 10^3$, respectively, which gives the ratio of the EHD number to Reynolds number squared $E_{\mathrm{hd}}/\mathrm{Re}^2 = 58$ (the calculation done for the discharge current per one nozzle $I_n = 8.3\ \mu$A, nozzle diameter $L_n = 1.5$ mm, air density $\rho = 1.205\ \mathrm{kg/m^3}$, air dynamic viscosity $\nu = 15 \times 10^{-6}\ \mathrm{m^2/s}$, ion mobility ($N_2^+$ in air) $\mu_i = 2.93 \times 10^{-4}\mathrm{m^2/Vs}$ [21], discharge area (nozzle area) $A = 1.77 \times 10^{-6}\ \mathrm{m^2}$, additional gas flow velocity at the nozzle $U_n = 0.59$ m/s). These Re and E_{hd} numbers show the crutial role of the EHD flow in the gas transport in the vicinity of the CDRS nozzle electrodes. It means that the additional gas flow hardly affects the ozone transport in the CDRS reactor, even in the vicinity of the CDRS electrode nozzles.

The comparison of the EHD force with the main flow inertia force in a 10-cm-wide region (from $x = -5$ to $x = +5$ cm; see Figs. 7 and 8) around the CDRS electrode, where the vortexes exist, gives the following. At a relatively low main flow velocity of 0.18 m/s, Reynolds and the EHD numbers are $\mathrm{Re} = 596$ and $E_{\mathrm{hd}} = 5.8 \times 10^6$, respectively, $E_{\mathrm{hd}}/\mathrm{Re}^2 = 16.4$. This shows a strong dominance of the EHD force over the inertial one. The increase in main flow velocity from 0.4 m/s to 0.6 m/s ($\mathrm{Re} = 1325$–1998, respectively) diminishes the importance of the EHD force ($E_{\mathrm{hd}} = 5.8 \times 10^6$, $E_{\mathrm{hd}}/\mathrm{Re}^2 = 3.3$–$1.5$, respectively). At a main flow velocity of 0.8 m/s, $\mathrm{Re} = 2650$, $E_{\mathrm{hd}} = 5.8 \times 10^6$, and $E_{\mathrm{hd}}/\mathrm{Re}^2 = 0.83$ (the calculations were carried out for $I_s = 150\ \mu$A, $L_s = 5$ cm, $A = 2 \times 10$ cm $\times$ 20 cm $= 0.04\ \mathrm{m^2}$, the other data as above). These numbers show that the EHD force should heavily influence the flow in the 10-cm-wide region around the CDRS electrodes even at a main flow velocity of 0.8 m/s. The PIV experiment confirmed this (Figs. 7 and 8). Therefore, we conclude that the EHD flow is the most important physical phenomenon responsible for the ozone transport into the upstream region of CDRS reactor.

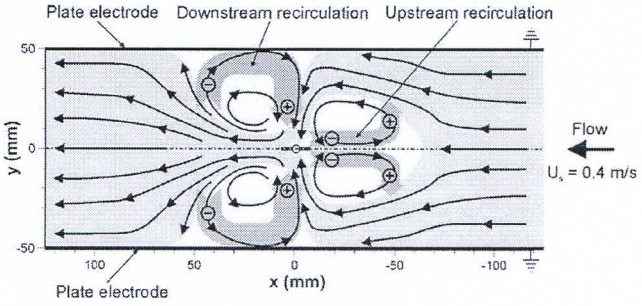

Fig. 9. Illustration showing the paths (dark grey) of the ozone transport in the CDRS reactor due to the EHD flows. Time-averaged velocity flow pattern was used.

D. Ozone Transport Model

As concluded above, the EHD force governs the ozone transport in the region where the strong EHD vortexes exist. A simple phenomenological model of the electrohydrodynamically induced ozone transport in the CDRS reactor is presented.

The model is one dimensional, i.e., all quantities are uniform in the y-z plane and any changes occur in the x direction (Figs. 1 and 2). It is assumed that the generation of O_3 molecules occurs around the CDRS electrode, i.e., around $x = 0$. The main gas flows with a constant mean velocity U_s, causing convection of O_3 molecules downstream. It is assumed that the EHD vortexes transport O_3 molecules upstream against the main flow, as shown by the dark grey paths in Fig. 9. The EHD vortexes remove O_3 molecules from the areas, marked as "$-$" in Fig. 9 (ozone sinks) and deliver them to the areas marked "$+$" (additional ozone sources).

In this model, it is assumed that O_3 molecules diffuse from the place of their origin upstream and downstream due to their density gradient. It is assumed that there is no loss of O_3 molecules in the reactor (on the walls or in the chemical reactions with the gas species). The turbulence mixing, transport due to temperature gradient, etc., apparently existing in the CDRS reactor, are neglected in this model. Also, the transport of O_3 molecules by the additional flow from the CDRS electrode nozzles is neglected, as justified in Section V-B.

In each point along the reactor, the time-dependence of O_3 number density is described by the molecule transport (5). In general, the source and sink terms S_n in (5) are a complex function of x. We simplify it by assuming a discrete distribution of the sources and sinks of O_3 molecules along the x axis. We assume that

$$S_n(x) = S_p^+(x) + S_{\mathrm{up}}^+(x) + S_{\mathrm{down}}^+(x) - S_{\mathrm{up}}^-(x) - S_{\mathrm{down}}^-(x) \tag{13}$$

where $S_p^+(x)$ is the production rate of O_3 molecules in the vicinity of the CDRS electrode; $S_{\mathrm{up}}^+(x)$ is the O_3 source on the rim of the upstream vortex (Fig. 9), resulting from the EHD transport; $S_{\mathrm{down}}^+(x)$ is the O_3 source resulting from the downstream EHD vortex which delivers O_3 molecules at around $x = 0$ mm; $S_{\mathrm{up}}^-(x)$ is O_3 sink resulting from O_3 molecule removal at around $x = 0$ mm by the upstream EHD vortex; and $S_{\mathrm{down}}^-(x)$ is O_3 sink on the rim of the EHD downstream vortex (Fig. 9).

It is assumed that the number density of O_3 molecules produced by the discharge in a unit length and in a unit time $S_p^+(x)$, and also the source and sink terms $S_{\text{up}}^+(x)$, $S_{\text{down}}^+(x)$, $S_{\text{up}}^-(x)$ and $S_{\text{down}}^-(x)$, are described by Gaussian functions. This means that all the sources and sinks are discretely but smoothly distributed along the x axis. The Gaussian profile width parameters w_i of the sources and sinks are, in general, different.

After inserting (13) into (5), (5) was solved numerically for the steady-state condition ($\partial n/\partial t = 0$). The solution fulfills the boundary condition: $\partial n/\partial x = 0$ for $L = \pm 50$ cm, where L is the distance from the CDRS electrode in the upstream and downstream directions.

In the calculations, we assumed that the diffusion coefficient of O_3 is equal to that of O_2 in air ($D = 0.2\ \text{cm}^2 \cdot \text{s}^{-1}$ [22]). The Gaussian profile width parameters w_i for the sources and sinks, varied in a reasonable range ($1\ \text{cm} < w_i < 4\ \text{cm}$) did not significantly influence the calculations. The intensities of the sources and sinks of O_3 were reasonably chosen to fit the experimental results. The positions of the sources and sinks of O_3 were inferred from the instantaneous velocity flow patterns, which give more objective information (than the time-averaged velocity flow pattern) on how deep O_3 molecules can be transported by the EHD vortex into the upstream reactor region. According to the instantaneous velocity flow patterns, the upstream O_3 source positions were chosen as follows: $x_{\text{up}} = -90, -80$, and -40 mm for main flow velocities of 0.3, 0.5, and 0.8 m/s, respectively. The total O_3 production in a unit time was estimated for each main gas velocity U_s from the relevant constant ozone concentration at the reactor exit, i.e., as found experimentally at $x > 30$ cm downstream (Fig. 6).

For comparison, we also calculated the ozone concentration distributions along the CRDS reactor without the EHD transport of ozone, i.e., when ozone was transported only by the diffusion and main gas convection (a diffusion-convection model).

Both results of the calculation of the ozone distribution along the CDRS reactor, i.e., with and without EHD transport, are presented in Fig. 6. The results (solid curves) which take into account the EHD transport of ozone fit reasonably with the experimental points for main flow velocities of 0.3, 0.5, and 0.8 m/s. The solid curves in Fig. 6 reflect the main features of the experimentally found ozone distributions along the CDRS reactor, i.e., they show the presence of ozone in the upstream region, ozone distribution maxima around the CDRS electrode, and constant ozone distribution at the reactor exit. On the contrary, these peculiarities of the ozone distribution were not revealed by the calculation when the EHD transport was neglected, i.e., using the diffusion-convection model (the dashed–dotted lines in Fig. 6). However, the phenomenological model presented in this paper failed to describe the ozone concentration distribution at $U_s = 0.18$ m/s. This is likely due to a different flow structure at a relatively low main flow velocity, which exhibits three-dimensional character.

Concluding, the EHD transport of ozone upstream against the main flow in the CDRS reactor, phenomenologically introduced into the ozone transport equation, made possible explanation the ozone distributions along the CDRS reactor, in particular the presence of ozone molecules far in the upstream direction.

VI. Summary and Conclusion

This investigation was aimed at the explanation of the experimental observations of Ohkubo *et al.* [4], [5] and Kanazawa *et al.* [6] that NO molecules were removed from the flue gas simulator not only in the discharge and downstream regions of the CDRS reactor, but also far in the upstream CDRS reactor region. The supposition made in [11] that the ozone molecules could be responsible for NO removal in the upstream region, due to the reaction

$$\text{NO} + \text{O}_3 \rightarrow \text{NO}_2 + \text{O}_2$$

was confirmed experimentally by Mizeraczyk *et al.* [12], who showed the presence of ozone molecules far in the upstream region of the CDRS reactor. However, until now it was uncertain how the ozone molecules could be transported upstream, against the main flow.

Since the transport of the ozone molecules by the diffusion and additional gas flow from the CDRS nozzle electrode could not explain the ozone presence in the upstream region of the CDRS reactor, it was expected that the EHD secondary flow is the dominant carrier of the ozone molecules into the upstream region.

The present PIV measurements of the velocity field in the CDRS reactor confirmed the existence of a strong EHD flow in the reactor. This EHD flow manifested itself as strong vortexes having a possibility to transport species upstream and downstream. The analysis of the conservation equations for the EHD flow in the CDRS reactor pointed out the EHD flow as the dominant factor capable of transporting the ozone molecules upstream. The EHD flow prevails over the diffusion, additional gas, and main gas flows. The simple model, in which the EHD transport of ozone against the main flow in the CDRS reactor was phenomenologicaly introduced, was able to reflect all peculiarities of the ozone distributions in the CDRS reactor, in particular the ozone presence in the reactor upstream. This all gives evidence that the EHD flow influences the ozone distribution in the CDRS reactor, resulting in the ozone presence far in the upstream CDRS reactor region.

The EHD forced transport of ozone molecules in the CDRS reactor, inferred by the present investigation, helps in a better understanding of the observations of Ohkubo *et al.* [4], [5] and Kanazawa *et al.* [6].

Another conclusion is that the EHD transport of the active species outside of the discharge zone can enhance the gaseous pollutant removal in the nonthermal plasma reactors. Hence, apart from the discharge zone, other regions of the reactor can be important for the processing of gaseous pollutants.

The presence of a strong EHD secondary flows should have an important impact on modeling and optimizing the plasma processes as well as designing the nonthermal plasma reactors. It means that not only the processes occurring in the corona streamer discharge zone should be taken into account when modeling the chemical kinetics of species in the nonthermal plasma reactors, but the modeling should also comprise processes outside the discharge zone. These processes may be brought about by the active species transport caused by the EHD secondary flow.

ACKNOWLEDGMENT

The authors would like to thank A. Nomoto, K. Urashima, N. J. Mason, J. D. Skalny, S. Pekarek, M. Simek, and F. Pontiga for valuable discussions and comments.

REFERENCES

[1] J. S. Chang, P. Lawless, and T. Yamamoto, "Corona discharge processes," *IEEE Plasma Sci.*, vol. 19, pp. 1152–1166, 1991.

[2] B. M. Penetrante, J. N. Bardsley, and M. C. Hsiao, "Kinetic analysis of nonthermal plasmas used for pollution control," *J. Appl. Phys.*, vol. 36, pp. 5007–5017, 1997.

[3] K. Urashima and J. S. Chang, "Removal of volatile organic compounds from air streams and industrial flue gases by nonthermal plasma technology," *IEEE Trans. Dielectrics Electric. Insulation*, vol. 7, pp. 602–614, 2000.

[4] T. Ohkubo, S. Kanazawa, Y. Nomoto, and J. Mizeraczyk, "Two-dimensional distribution of NO by LIF technique in a corona radical shower reactor during NO_x removal processing," in *Proc. 35th Annual Meeting IEEE Industry Applications Soc.*, vol. 1&2, Rome, Italy, 2000, pp. 864–867.

[5] T. Ohkubo, T. Ito, Y. Shuto, S. Akamine, S. Kanazawa, Y. Nomoto, and J. Mizeraczyk, "Streamer corona discharge induced by laser pulses during LIF measurements in a dc nonthermal plasma reactor for NO oxidation," *J. Adv. Oxid. Tech.*, vol. 5, no. 2, pp. 129–134, 2002.

[6] S. Kanazawa, Y. Shuto, N. Sato, T. Ohkubo, Y. Nomoto, J. Mizeraczyk, and J. S. Chang, "Two-dimensional imaging of NO density profiles by LIF technique in a pipe with nozzles electrode during NO treatment," *IEEE Trans. Indust. Applicat.*, vol. 39, pp. 333–339, June 2003.

[7] L. B. Loeb, *Electrical Coronas*, C. A. Berkeley and E. Coronas, Eds: Univ. California Press, 1965, pp. 402–407.

[8] T. Yamamoto and H. R. Velkoff, "Electrohydrodynamics in an electrostatic precipitator," *J. Fluid Mech.*, vol. 108, pp. 1–18, 1981.

[9] P. Atten, F. M. J. Mccluskey, and A. C. Lahjomri, "The electrohydrodynamic origin of turbulence in electrostatic precopitators," *IEEE Trans. Indust. Applicat.*, vol. 23, pp. 705–711, 1987.

[10] J. Mizeraczyk, M. Kocik, J. Dekowski, M. Dors, J. Podliński, T. Ohkubo, S. Kanazawa, and T. Kawasaki, "Measurements of the velocity field of the flue gas flow in an electrostatic precipitator model using PIV method," *J. Electrostatics*, vol. 51–52, pp. 272–277, 2001.

[11] J. Mizeraczyk, J. Dekowski, J. Podliński, M. Dors, M. Kocik, J. Mikielewicz, T. Ohkubo, and S. Kanazawa, "Images of electrohydrodynamic flow velocity field in a dc positive polarity needle-to-plate nonthermal plasma reactor," *IEEE Trans. Plasma Sci*, vol. 30, pp. 164–165, Feb. 2002.

[12] J. Mizeraczyk, J. Podliński, M. Dors, M. Kocik, T. Ohkubo, S. Kanazawa, and J.S. Chang, "Electrohydrodynamic transport of ozone in a corona radical shower nonthermal plasma reactor," *Czech. J. Phys., Suppl. D*, vol. 52, pp. D413–D420, 2002.

[13] T. Ohkubo, S. Kanazawa, Y. Nomoto, J. S. Chang, and T. Adachi, "NO_x removal by a pipe with nozzle-plate electrode corona discharge system," *IEEE Trans. Indust. Applicat.*, vol. 30, no. 4, pp. 856–861, 1994.

[14] S. Kanazawa, J. S. Chang, G. F. Round, G. Sheng, T. Ohkubo, Y. Nomoto, and T. Adachi, "Removal of NO_x from flue gas by corona discharge activated methane radical showers," *J. Electrostatics*, vol. 40&41, pp. 651–656, 1997.

[15] K. Urashima, S. J. Kim, and J. S. Chang, "The scale-up and economic evaluation of nonthermal plasma technology for coal fired power plant exhaust gas emission control," *J. Adv. Oxid. Tech.*, vol. 6, pp. 123–131, 2003.

[16] A. C. Gentile and M. J. Kushner, "Reaction chemistry and optimization of plasma remediation of N_xO_y from gas streams," *J. Appl. Phys.*, vol. 78, pp. 2074–2085, 1995.

[17] J. J. Lowke and R. Morrow, "Theoretical analysis of removal of oxides of sulphur and nitrogen in pulsed operation of electrostatic precipitators," *IEEE Trans. Plasma Sci.*, vol. 23, pp. 661–671, 1995.

[18] E. A. Filimonova, R. H. Amirov, H. T. Kim, and I. H. Park, "Comparative modeling of NO_x and SO_2 removal from pollutant gases using pulsed-corona and silent discharges," *J. Phys. D: Appl. Phys.*, vol. 33, pp. 1716–1727, 2000.

[19] K. Yan, T. Yamamoto, S. Kanazawa, T. Ohkubo, Y. Nomoto, and J. S. Chang, "Control of flow stabilized positive corona discharge modes and NO removal characteristics in dry air by CO_2," *J. Electrostatics*, vol. 46, pp. 207–219, 1999.

[20] J. S. Chang and A. Watson, "Electromagnetic hydrodynamics," *IEEE Trans. Dielectrics Electric. Insulation*, vol. 5, no. 1, pp. 871–895, 1994.

[21] J. S. Chang and A. Kwan, "Modeling of dry air chemistry in a coaxial wire-pipe negative corona discharge," in *Proc. EESA-IEJ Joint Symp. Electrostatics 1998*, Palo Alto, CA, 1998, pp. 390–408.

[22] B. Eliasson, M. Hirth, and U. Kogelschatz, "Ozone synthesis from oxygen in dielectric barrier discharges," *J. Phys. D: Appl. Phys.*, vol. 20, pp. 1421–1437, 1987.

Jaroslaw Dekowski received the M.Sc. degree in applied physics in fluid mechanics from the Technical University of Gdańsk, Gdańsk, Poland, in 2002.

He works as an Assistant Researcher at the Institute of Fluid Flow Machinery, Polish Academy of Sciences, Gdańsk. His research interests include fluid and particle flows in electrostatic precipitators, electrohydrodynamics, PIV measurement technique, and numerical fluid dynamics.

Jerzy Mizeraczyk received the M.Sc. degree from the Technical University of Gdańsk, Gdańsk, Poland, in 1966 and the Ph.D. degree from the University of Gdańsk in 1975.

He was a Fellow of the Japan Society for the Promotion of Science at Nagoya University, Japan, for the A. von Humboldt Foundation, and for the H. Hertz Foundation at Ruhr University, Bochum, Germany. He was a Visiting Senior Researcher at the Chalmers University of Technology, Göteborg, Sweden, and at McMaster University, Hamilton, ON, Canada. He also was a Full Professor at Oita University, Japan. He is currently the Head of the Centre for Plasma and Laser Engineering, Institute of Fluid-Flow Machinery, Polish Academy of Sciences, Gdańsk. He was a Co-Director of two European Community Copernicus Projects and one NATO "Science for Peace Programme" Project. He has worked in the areas of plasma physics, dc, pulsed, RF, and MW discharges, gas lasers and their applications, and plasma chemistry for environmental technologies. He has authored more than 100 published refereed papers and presented more than 100 conference papers on these topics.

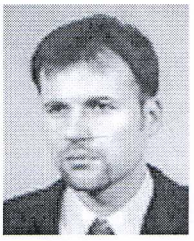

Marek Kocik was born in Warsaw, Poland, in 1970. He received the M.Sc. degree in experimental physics from University of Gdańsk, Gdańsk, Poland, in 1996 and the Ph.D. degree from the Institute of Fluid Flow Machinery, Polish Academy of Sciences, Gdańsk, in 2002.

He is presently an Associate Researcher for the Polish Academy of Sciences. His research interests include laser applications to micromachining, laser flow diagnostics, and laser spectroscopy. He has authored 15 published refereed papers and presented more than 40 conference papers on these topics. Since 2003, he has held a postdoctoral position in the Department of Electrical and Electronic Engineering, Oita University, Oita, Japan.

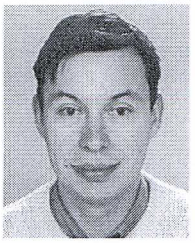

Mirosław Dors received the M.S. degree in chemistry from the Technical University of Gdańsk, Gdańsk, Poland, and the Ph.D. degree in mechanics from the Institute of Fluid Flow Machinery, Polish Academy of Sciences, Gdańsk, in 1993 and 2000, respectively.

He is currently with the Institute of Fluid Flow Machinery, Polish Academy of Sciences, Gdańsk. He is co-author of over 70 scientific papers and conference communications concerning experimental and modeling contributions to the technology of nonthermal plasma removal of NO_x and hydrocarbons from flue gases, and decomposition of high-concentration hydrocarbons, chlorinated hydrocarbons, and freons using microwave torch plasma at atmospheric pressure.

Janusz Podliński received the M.Sc. degree in electronics and telecommunications from the Technical University of Gdańsk, Gdańsk, Poland, in 2001.

He currently works as an Assistant Researcher at the Institute of Fluid Flow Machinery, Polish Academy of Sciences, Gdańsk. His research interests include fluid and particle flows in electrostatic precipitators and nonthermal plasma reactors, electrohydrodynamics, and PIV measurement techniques.

Seiji Kanazawa (M'91) was born in Usuki, Oita, Japan, on December 7, 1961. He received the B.E., M.E., and Ph.D. degrees from Kumamoto University, Kumamoto, Japan, in 1985, 1987, and 1990, respectively.

Since 1990, he has been with Oita University, Oita, where he is presently an Associate Professor in the Department of Electrical and Electronic Engineering. His research interests include the areas of applied electrostatics, air pollution control, plasma technologies, plasma diagnosis, and eco-material processing using lasers.

Dr. Kanazawa is a member of the Institute of Electrical Engineers of Japan, the Institute of Electronics, Information, and Communication Engineers of Japan, the Institute of Electrostatics Japan, and the Japan Society of Applied Physics.

Toshikazu Ohkubo (M'86) was born in Beppu, Japan, in 1948. He received the B.E., M.E., and D.E. degrees from Kyushu University, Fukuoka, Japan, in 1972, 1975, and 1986, respectively.

From 1975 to 1987, he was a Research Associate in the Department of Electrical Engineering, Oita University, Oita, Japan. From 1988 to 1989, he was a Visiting Research Fellow at McMaster University, Hamilton, ON, Canada. He became an Associate Professor in 1987 and a Professor in 1995 in the Department of Electrical and Electronic Engineering, Oita University. His research interests include NO_x removal by corona-discharge-induced plasmas, electrohydrodynamics, NO measurement by laser-induced fluorescence, and thin-film preparation by pulsed-laser deposition for fuel cells.

Dr. Ohkubo is a member of the Institute of Electrical Engineers of Japan, Institute of Electrostatics Japan, and the Japan Society of Applied Physics.

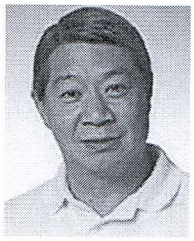

Jen-Shih Chang (M'90–SM'96) received the B. Eng. and M. Eng. degrees in electrical engineering from Musashi Institute of Technology, Tokyo, Japan, and the Ph.D. degree in experimental space sciences from York University, Toronto, ON, Canada.

From 1973 to 1974, he was a Researcher at the Centre de Recherches en Physique de l'Environment, CNRS, France. From 1975 to 1979, he was a Project Scientist/Assistant Professor with the Department of Physics and Center for Research in Experimental Space Sciences, York University. From 1979 to 1986, he was an Assistant Professor/Associate Professor with the Department of Engineering Physics, McMaster University, Hamilton, ON, Canada. From 1985 to 1996, he was a Visiting Professor at Musashi Institute of Technology, Tokyo Denki University, the University of Tokyo, University of Seville, Joseph Fourier University, University of Poitiers, Oita University, and Tokyo University of Agriculture and Technology. Since 1987, he has been a Professor at McMaster University and is involved in research on applied electrostatics, lightning, air pollution control, and solid and liquid waste destruction plasma technologies.

Dr. Chang is currently Chair of the Electrohydrodynamics Technical Committee of the IEEE Dielectrics and Electric Insulation Society.